

Incorporating Kinematic Wave Theory into a Deep Learning Method for High-Resolution Traffic Speed Estimation

Bilal Thonnam Thodi^{1,2}, Zaid Saeed Khan^{†1,2}, Saif Eddin Jabari^{1,2}, and Mónica Menéndez^{1,2}

¹New York University Tandon School of Engineering, Brooklyn NY, U.S.A.

²New York University Abu Dhabi, Saadiyat Island, P.O. Box 129188, Abu Dhabi, U.A.E.

[†]Corresponding author. Email: zaid.khan@nyu.edu

Abstract. We propose a kinematic wave based Deep Convolutional Neural Network (Deep CNN) to estimate high resolution traffic speed dynamics from sparse probe vehicle trajectories. To that end, we introduce two key approaches that allow us to incorporate kinematic wave theory principles to improve the robustness of existing learning-based estimation methods. First, we use an anisotropic traffic-based kernel for the CNN. This kernel is designed to explicitly take forward and backward traffic wave propagation characteristics into account during reconstruction in the space-time domain. Second, we use simulated data for training the CNN. This implicitly imposes physical constraints on the patterns learned by the CNN, providing an alternate, unrestricted way to integrate complex traffic behaviors into learning models. We present the speed fields estimated using the anisotropic kernel and highlight its advantages over its isotropic counterpart in terms of predicting shockwave dynamics. Furthermore, we test the transferability of the trained model to real traffic by using two datasets: the Next Generation Simulation (NGSIM) program and the Highway Drone (HighD) dataset. Finally, we present an ensemble version of the CNN that allows us to handle multiple (and unknown) probe vehicle penetration rates. The results demonstrate that anisotropic kernels can reduce model complexity while improving the correctness of the estimation, and that simulation-based training is a viable alternative to model fitting using real-world data. This suggests that exploiting prior traffic knowledge adds value to learning-based estimation methods, and that there is great potential in exploring broader approaches to do so.

Keywords: Traffic state estimation, traffic dynamics, data imputation, convolutional neural networks, anisotropic traffic flow, kinematic wave theory.

1 Introduction

Traffic management agencies use a variety of monitoring and control tools to ensure the safe and efficient operation of network road traffic. To meet their operational goals, agencies employ tools that identify disturbances and deploy effective control strategies in real time [39]. However, this requires accurate and timely knowledge of traffic conditions over the entire network, which is currently not possible given the limited sensory instrumentation in most (if not all) cities today. Fixed sensors are expensive and tend to be sparsely installed, offering limited spatial coverage. Data from mobile sensors are expected to become more widely available than data from point sensors, but remain

extremely limited in practice; their sparsity is temporal. To address such data sparsity (spatially or temporally), we need appropriate mechanisms that fill the gaps in the traffic observations. These are known as *traffic state estimation* (TSE) tools [44]. TSE is a critical precursor to a number of real-time traffic control strategies with either conventional vehicles or a mix with connected and autonomous vehicles [27, 39, 61]. Such strategies include, but are not limited to, ramp metering, perimeter control, traffic signal control, and vehicle routing [11, 25, 32, 45, 62, 67]. Existing TSE methods are categorized and discussed below, along with their advantages and drawbacks.

TSE approaches can be broadly divided into two categories: model-based and data-driven [44]. The former ap-

proach adopts a mathematical model of traffic flow such as the first-order Lighthill-Whitham-Richards (LWR) model [31, 42] or one of its many higher-order extensions, like the Aw-Rascle-Zhang (ARZ) model [2, 64]. The TSE approaches in this category often assimilate their chosen traffic flow model with observations using Kalman filters [3, 4, 9, 15–17, 37, 53, 58, 63, 68]. The principal advantage of using a traffic flow model is that it ensures that estimation process respects basic traffic principles. Furthermore, they have explanatory power in the sense that they provide insights into the steps involved in the estimation and its performance. However, these methods also have some drawbacks. First, the models themselves are based on simplifying assumptions of traffic physics that can lead to numerical bias in the model when the assumptions are not met. Second, approximation errors can arise from the data assimilation techniques used in TSE. For instance, it is common to linearize a non-linear traffic model around the current state to fit into the recursive estimation framework while filtering. When the linear approximation is taken around the capacity region, the errors can be significant, e.g., the model can predict free-flow when the facility is congested [44, 63].

The other category of TSE approaches use data-driven techniques, namely statistical/machine learning methods. These techniques rely on finding patterns in large volumes of (historical) traffic data during training. They continue to gain popularity over model-based approaches in TSE, mainly because the large amounts of detailed traffic data and computational power they require has become more readily available in recent years. The most common type of machine learning tool used in data-driven approaches is deep learning (DL), specifically deep neural networks (DNNs) [5, 12, 20, 24, 34, 40, 56]. Other techniques include support vector machines [57], case based reasoning [21], random forests [13], decision trees [35], gradient boosting [65], kernel regression [59], principal component analysis [26], and matrix factorization methods [29, 30]. The estimation results from data-driven methods are often reported to be more accurate than model-based approaches. However, these methods also have shortcomings. Being purely data-driven, the resulting models are agnostic to the physics of traffic flow, which means that they cannot guarantee that the results will be physically feasible. Furthermore, the generalizability of the models is often weak and depends heavily on the amount and variety of data used for training. Perhaps the biggest limitation of these methods, particularly as seen by traffic researchers, is that they lack interpretability. They are often referred to as “black boxes” and criticized by some traffic experts for the difficulty of obtaining insight from the building blocks

of the models.

We aim to develop methodology that combines desirable features of both categories, namely the combination of domain knowledge with representational power. This will ensure accurate and interpretable results, model parsimony, and reduced data requirements. Some recent works along these lines include [18, 19, 43, 60, 66]. In the deep learning literature, there is a new paradigm called “Physics-informed deep learning” [41], where the governing physical dynamical equations (in the form of PDEs or ODEs) are incorporated into the architecture or cost function of the DNN, acting as a regularizer. This is already being explored in the context of TSE in [14, 33, 46]. In these works, the authors demonstrate that these physics informed regularizers reduce the space of feasible solutions and learn solutions that are consistent with the chosen models with limited data.

We propose an addition to this nascent literature on hybrid data-driven TSE methods that incorporate traffic domain knowledge. Our speed reconstruction method uses a Deep Convolutional Neural Network (Deep CNN) that is trained off-line and can then be applied in real-time. The Deep CNN takes as input sparse vehicle trajectory measurements and outputs a high-resolution speed field over a given space-time domain. We incorporate traffic-specific features into the learning model in two ways, which are described below.

First, the naïve isotropic kernels in the Deep CNN model are modified to capture the wave propagation characteristics of free-flowing and congested traffic, in accordance with the kinematic wave theory (KWT) of traffic flow [38]. We develop a Deep CNN with *anisotropic kernels* designed to consider space-time inputs that are in the direction of feasible traffic waves (forward waves in free-flow and backward waves in congested traffic) for the traffic speed interpolation. As a result, we can reduce the effective number of kernel parameters and, hence, the Deep CNN model’s complexity. Further, guiding the CNN to consider only the relevant spatio-temporal input points results in feasible reconstruction of shockwaves in the estimated speed fields.

Second, we train our Deep CNN model using simulated traffic data. This approach complements the existing physics-informed learning methods whereby, instead of explicitly incorporating the governing dynamical equation into the model architecture, we take an empirical distribution of the given traffic flow model and use it to train the Deep CNN. The empirical distribution is a surrogate representation of the traffic physics underlying the simulation model. This is a more broader approach to incorporate the governing physics as it is easy to generate data correspond-

ing to complex traffic behaviors than integrating them into the learning-model architecture. We demonstrate this by training the Deep CNN model with data generated from a microscopic traffic simulator, which consists of behavioral car-following, lane-changing and gap-acceptance models, and then test with real-world data having similar traffic characteristics. A natural trade-off of this approach is that the learning model doesn't capture the exact physical traffic dynamics, but can incorporate a wide range of complex traffic behaviors. Similar methods have been explored in the context of automated systems such as robotic controls, object detection, etc., whereby researchers use high-fidelity simulators or synthetic data to train deep neural network models instead of using real-world data [47, 51].

To summarize, the contributions of this paper are:

1. We develop an anisotropic kernel design for CNNs following the wave propagation characteristics of traffic flow. The applications include traffic state estimation, traffic prediction, and data imputation. We also suggest an optimization procedure to learn the optimal weights for the anisotropic kernels.
2. We propose to use simulated traffic data for fitting the anisotropic Deep CNN model and test its performance on real-world datasets.
3. We reconstruct high resolution (10 meters \times 1 second) traffic speed fields from limited probe vehicle data (with 5% penetration levels) using the anisotropic Deep CNN. We show sample reconstructions of real-world data from multiple sources.
4. We extend our reconstruction methodology to handle unknown probe vehicle penetration rates by introducing an ensemble version of our Deep CNN model.

The rest of the paper is structured as follows. We present the speed reconstruction problem setting, the anisotropic kernel design, and the optimization procedure in Section 2. We then describe the training data generation and the training experiments in Section 3. In Section 4, we present reconstruction results, compare the anisotropic CNN with the naïve isotropic variant, discuss the transferability of the reconstruction model to real-world freeway traffic, and explore the sensitivity of the results to different probe vehicle penetration levels. Finally, we summarize our contributions in Section 5.

2 Estimation Methodology

2.1 Speed reconstruction problem

A space-time domain $\mathcal{D} = \mathcal{X} \times \mathcal{T}$ representing a given road section is discretized into homogeneous segments $x_i \subset \mathcal{X}$ and time intervals $t_i \subset \mathcal{T}$, such that $\cup_i x_i = \mathcal{X}$ and $\cup_i t_i = \mathcal{T}$. Let $V(x, t)$ denote the value of the macroscopic speed field in a cell $(x, t) \in \mathcal{D}$. We use the cell size $|x|$ closer to the length of a vehicle and $|t|$ of the order of seconds (smaller than what existing estimation methods use [44]) to enable high-resolution speed field reconstruction. Probe vehicles (PVs) provide local speed measurements $\{V^p(x_i^p, t_i^p)\}$ for some cells in \mathcal{D} ; we represent this partial information by the tensor \mathbf{z}^p . We assume sparse observation settings, where only a few cells (e.g., 5-10%) in \mathbf{z}^p have speed information. We denote by \mathbf{z}^f a tensor of estimates of the complete speed field $V(x, t)$ for the entire space-time domain \mathcal{D} . The reconstruction problem can be formally stated as learning a mapping function $g : \mathbf{z}^p \mapsto \mathbf{z}^f$.

The speed field $V(x, t)$ in each cell of the input tensor \mathbf{z}^p is encoded using a three-dimensional RGB array (with domain $\{1, \dots, 255\}$) instead of a one-dimensional speed value. This is to differentiate cells occupied with a stopped vehicle (i.e., with $V(x, t) = 0$) from empty cells. The output tensor \mathbf{z}^f represents the complete macroscopic speed field over the domain \mathcal{D} and can be encoded using the one-dimensional speed values. Thus, we have, $\mathbf{z}^p \in \{1, \dots, 255\}^{|\mathcal{X}| \times |\mathcal{T}| \times 3}$ and $\mathbf{z}^f \in \mathbb{R}_{\geq 0}^{|\mathcal{X}| \times |\mathcal{T}|}$.

2.2 Deep Convolutional Neural Network (Deep CNN) reconstruction model

We use a Deep CNN model similar to the one in [5] to represent the mapping function g . The model architecture is shown in Fig. 1. It comprises an encoder g_{enc} and a decoder g_{dec} , each consisting of three CNN layers. Each CNN layer is composed of a 2D convolution operation, a non-linear activation operation called ReLU (Rectified Linear Unit), and a down-sampling operation called max-pooling (up-sampling operation called nearest neighbor in case of g_{dec}). The CNN takes the input \mathbf{z}^p , passes it through the hierarchical convolution layers, and outputs the reconstructed speed field \mathbf{z}^f .

The discrete convolution using local kernels forms the basis of the reconstruction. In a given CNN layer l , a convolution operation calculates the activation in a cell (x, t) as a weighted sum of cell activations observed in the previous layer $(l - 1)$:

$$\begin{aligned} \mathbf{z}^{(l)}(x, t, \chi) &= \mathbf{z}^{(l-1)}(\cdot, \cdot, \chi) * \Theta^{(l)}(\cdot, \cdot) \\ &= \sum_{(x_j, t_j) \in I_{\text{iso}}} \mathbf{z}^{(l-1)}(x_j, t_j, \chi) \Theta^{(l)}(x_j, t_j), \quad (1) \end{aligned}$$

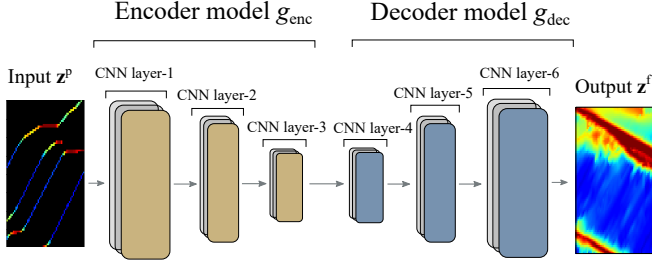


FIGURE 1: The architecture of the Deep CNN (speed reconstruction model).

where $\mathbf{z}^{(l)}(x, t, \chi)$ is the feature map value in layer l associated with cell (x, t) and color channel $\chi \in \{1, 2, 3\}$, $\Theta^{(l)}(\cdot, \cdot) \in \mathbb{R}^{|\mathcal{X}| \times |\mathcal{T}|}$ is the kernel (matrix), which is identical for all cells. $\Theta^{(l)}(x_j, t_j)$ on the right-hand side, an element of the kernel matrix, determines the extent to which neighboring cell $(x_j, t_j) \in I_{\text{iso}}$ is correlated with the subject cell (x, t) . Hereafter, we simply write Θ to represent the entire kernel, and drop the (\cdot, \cdot) .

The feature map value in cell (x, t) can be considered as equivalent to (or some function of) the speed field $V(x, t)$ in that cell. Then, operation (1) simply says: the speed in cell (x, t) is a weighted interpolation of speeds observed in its immediate surrounding cells. The extent of local cell influence I_{iso} is depicted visually on the space-time plane in Fig. 2(a). Each kernel in a layer l represents a different weighting function; together, the kernels learn to identify different traffic features.

2.3 Anisotropic kernel design for Deep CNN

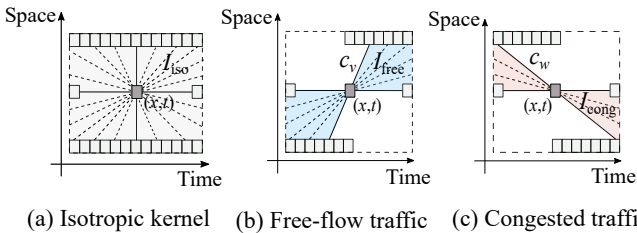


FIGURE 2: Space-time correlations modeled by the isotropic kernel of the convolution operation, and that in the real traffic (free-flow and congested).

The isotropic kernel shown in Fig. 2(a) says that the speed in cell (x, t) is correlated with the speeds observed *anywhere* in the shaded rectangular region I_{iso} . This assumes that a speed variation (such as that caused by slow-downs or speed-ups) at (x, t) can propagate at unbounded

velocities in the space-time plane. However, this is not true in real traffic. In real traffic, (i) the speed/density variations propagate at finite velocities that are less than or equal to the free-flowing vehicle speed, and (ii) vehicles respond (predominantly) to frontal stimuli with a delay (approximately equal to the reaction time of driver). The former condition is called hyperbolicity and the latter is called anisotropy. Hyperbolicity is a necessary but not sufficient condition for anisotropy in traffic flow models [7, 49, 55]. The use of local kernels (i.e., kernel dimensions \ll the dimension of space-time plane) captures the hyperbolicity property, whereas anisotropy can be captured by modifying the kernel shape as discussed below.

The actual propagation velocity of speed variations depends on the traffic state (i.e., speed or density). We assume here that the traffic at any point in the space-time plane is either in free-flow or is congested. Then, a speed variation in cell (x, t) propagates downstream (i.e., in the direction of traffic) in free-flowing traffic and upstream (i.e., in the opposite direction of traffic) in congested traffic. This is an empirically and theoretically established feature of traffic [6, 8, 38, 48, 50]. Thus, the extent of the space-time plane correlated with cell (x, t) depends on whether the traffic state is free-flow or congested. The respective correlated regions are shown in Fig. 2(b) and Fig. 2(c) as shaded areas I_{free} and I_{cong} .

The regions I_{free} and I_{cong} are bounded by the free flow traffic speed c_v and the backward shockwave velocity c_w [49, 55], respectively. The speed in cell (x, t) influences the region I_{free} downstream, and the region I_{cong} upstream. Likewise, the regions I_{free} upstream and I_{cong} downstream influence the speed in cell (x, t) . In summary, the speed predicted in cell (x, t) is correlated with the speeds observed anywhere in $I_{\text{free}} \cup I_{\text{cong}}$. We use this knowledge of space-time correlations in designing an alternate and more *correct* kernel (in the traffic sense) for the Deep CNN model in Fig. 1. We refer to this as the *anisotropic kernel*, and represent it by the tensor $\Theta_{\text{ani}} = [\Theta_{\text{ani}}^{(l)}]_l$. The corresponding convolution operation is slightly modified from (1) as,

$$\begin{aligned} \mathbf{z}^{(l)}(x, t, \chi) &= \mathbf{z}^{(l-1)}(\cdot, \cdot, \chi) * \Theta_{\text{ani}}^{(l)} \\ &= \sum_{(x_j, t_j) \in I_{\text{ani}}} \mathbf{z}^{(l-1)}(x_j, t_j, \chi) \Theta_{\text{ani}}^{(l)}(x_j, t_j), \end{aligned} \quad (2)$$

where the effective influence region is defined as $I_{\text{ani}} := I_{\text{free}} \cup I_{\text{cong}}$. This way, we direct the convolution operator to consider only that portion of the space-time plane which is relevant for the speed interpolation according to traffic physics.

In this paper, we propose a specific anisotropic kernel design, whose influence region is further restricted, moti-

vated by empirical observations: (i) congested traffic has a very narrow range of wave propagation velocities (such that they can be regarded as almost constant), and (ii) free-flow traffic wave propagation velocities are limited within the maximum and minimum desired vehicle speeds [38, 48–50, 55]. The anisotropic kernel design to replace the isotropic kernel (from Fig. 1) is illustrated in Fig. 3. We create two kernels, one each for free-flowing and congested traffic. The influence region I_{free} contains all the cells passing and bounded the maximum (c_v^{max}) and minimum (c_v^{min}) desired vehicle speeds. This is relevant for heterogeneous traffic where the desired speed distribution has a wide range. The free-flow traffic kernel is shown in Fig. 3(a). The influence region for congested traffic, I_{cong} , contains only those cells passing through the backward propagating shockwave velocity c_w ; see Fig. 3(b). The proposed anisotropic kernel is a superposition of the free-flow and congested kernel. This is shown in Fig. 3(c). The corresponding isotropic kernel is shown in Fig. 3(d) for comparison. One can see that the anisotropic design requires 50% fewer parameters than its isotropic variant for a 7×7 kernel. Note here that the speeds $\{c_v^{\text{max}}, c_v^{\text{min}}, c_w\}$ are inputs based on the traffic characteristics of the road section.

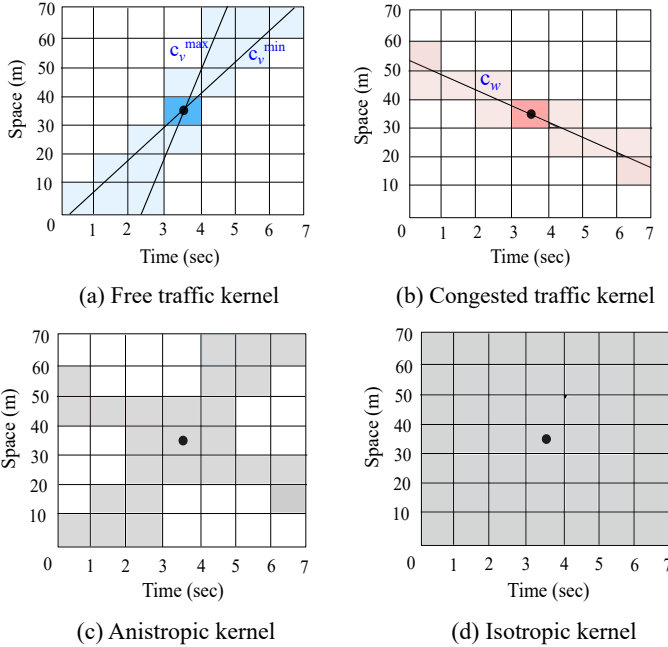


FIGURE 3: The anisotropic kernel design for a 7×7 CNN kernel. The naïve isotropic kernel is also shown here for comparison. Parameters used: $c_v^{\text{max}} = 100$ kmph, $c_v^{\text{min}} = 60$ kmph and $c_w = 18$ kmph.

The proposed anisotropic kernel design is similar to Treiber and Helbing’s adaptive smoothing method for speed interpolation [48] except that: (a) we consider a range of wave propagation velocities in free-flowing traffic instead of a constant value, (b) the weights in the kernel are not set a priori as in [48] but learned from data, and (c) the actual speed predicted is a combination of several anisotropic kernels as opposed to a single anisotropic kernel.

2.4 Learning anisotropic kernels

We use anisotropic kernels in all layers of the Deep CNN model in Fig. 1. The optimal weights Θ_{ani}^* for the anisotropic kernel are obtained from the following constrained optimization problem:

$$\Theta_{\text{ani}}^* := \arg \min_{\Theta \in \mathbb{R}^{|\mathcal{X}| \times |\mathcal{T}| \times L}} \{ \mathcal{L}(\mathbf{z}^f, g(\mathbf{z}^p, \Theta)) : \mathbb{1}_{\text{ani}} \odot \Theta = \mathbf{0} \}, \quad (3)$$

where $g(\mathbf{z}^p, \Theta) : \{0, \dots, 255\}^{|\mathcal{X}| \times |\mathcal{T}| \times 3} \rightarrow \mathbb{R}_{\geq 0}^{|\mathcal{X}| \times |\mathcal{T}|}$ is the mapping function (i.e., the Deep CNN) with the kernel parameterization Θ made explicit (i.e., g performs the mapping $\mathbf{z}^p \mapsto \mathbf{z}^f$), $\mathbb{1}_{\text{ani}}$ is a binary tensor of the same dimension as Θ with values of 0 for cells corresponding to the anisotropic influence cell region I_{ani} , e.g., the shaded cells in Fig. 3(c), and 1 elsewhere (\odot is the Hadamard product). The loss function \mathcal{L} captures any discrepancies between the reconstructed and true speed fields, e.g., the squared ℓ_2 distance (the squared error):

$$\mathcal{L}(\mathbf{z}^f, g(\mathbf{z}^p, \Theta)) = \|\mathbf{z}^f - g(\mathbf{z}^p, \Theta)\|_2^2. \quad (4)$$

The constrained optimization problem (3) can be solved using iterative schemes which can handle feasibility constraints, such as the projected gradient descent. In each iteration i , the updates are calculated as follows:

$$\Theta_{\text{ani}}^{i+1} := P_{I_{\text{ani}}}(\Theta_{\text{ani}}^i - \gamma^i G(\Theta_{\text{ani}}^i)), \quad (5)$$

where $\gamma_i > 0$ is the step size (or learning rate) in iteration i and $G(\Theta_{\text{ani}}^i)$ is a gradient tensor (descent direction) at Θ_{ani}^i . The operator $P_{I_{\text{ani}}}$ assigns zeros to elements of $\Theta_{\text{ani}}^i - \gamma^i G(\Theta_{\text{ani}}^i)$ corresponding to cells that lie outside of I_{ani} , thereby ensuring feasibility of the solutions.

2.5 Definition of macroscopic speed field

An important auxiliary task is to define the “true” speed field which the Deep CNN model uses as the “ground truth” for evaluating the quality of the estimation. This is achieved by *translating* the set of *all* vehicle trajectories (not just PVs) into a speed field $V(x, t)$. The commonly

used generalized definition of macroscopic speeds [10] results in $V(x, t) = 0$ for some cells due to the fine mesh size we use. Therefore, we propose a simple interpolation method for this purpose instead. Our method interpolates the speeds over the road cells at a fixed time according to:

$$V(x, t) = \begin{cases} V_{\text{up}}w + V_{\text{dn}}(1 - w), & \text{if } (x - x_{\text{up}}) < l_{\text{up}} \\ & \text{and } (x_{\text{dn}} - x) < l_{\text{dn}} \\ V_{\text{up}}w + V_{\text{max}}(1 - w), & \text{if } (x - x_{\text{up}}) < l_{\text{up}} \\ & \text{and } (x_{\text{dn}} - x) > l_{\text{dn}} \\ V_{\text{dn}}w + V_{\text{max}}(1 - w), & \text{if } (x - x_{\text{up}}) > l_{\text{up}} \\ & \text{and } (x_{\text{dn}} - x) < l_{\text{dn}} \\ V_{\text{max}}, & \text{otherwise,} \end{cases} \quad (6)$$

where V_{max} is the highest free-flow speed (or speed limit of the highway section), V_{dn} (resp. V_{up}) is the speed of the downstream (resp. upstream) vehicle, x_{dn} (resp. x_{up}) is the position of the cell containing the downstream (resp. upstream) vehicle, l_{dn} (resp. l_{up}) is the length of spatial interaction downstream (resp. upstream) of (x, t) , and $w \in [0, 1]$ is a weight assigned to the respective speed values.

Equation (6) reads as: the speed field $V(x, t)$ in cell (x, t) is a weighted combination of three speed values – the speeds V_{dn} and V_{up} of vehicles immediately downstream and upstream of the cell (x, t) , and the maximum highway speed V_{max} . The downstream vehicle has an effect only if it is within the downstream interaction range l_{dn} from the cell (x, t) , and analogously for the upstream vehicle. The weight w captures this interaction effect and is inversely proportional to the relative distance from the vehicle downstream $(x_{\text{dn}} - x)$ or upstream $(x - x_{\text{up}})$. The spatial interaction lengths are chosen to satisfy $l_{\text{up}} > l_{\text{dn}}$, to reflect the asymmetrically greater influence of frontal interaction.

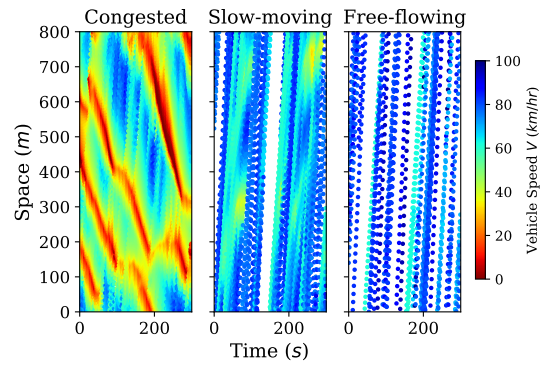
3 Data and Training

3.1 Training data generation

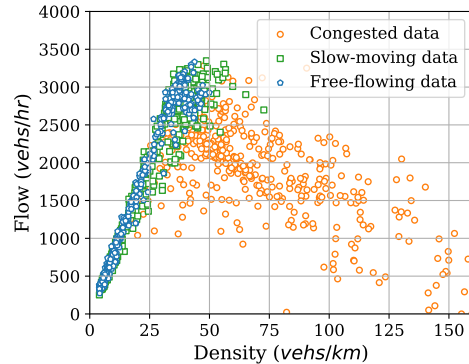
To generate data for training the CNN model, we simulate a freeway segment using a commercial microscopic traffic simulator. The simulated segment corresponds to the *E-22 Abu Dhabi-Al Ain road, UAE* (2 miles in length and 3 lanes wide), and includes an entry and exit ramp to a nearby suburban region. The simulation model is calibrated with general traffic behavior, for instance, prioritizing through movements, appropriate yielding gaps for on-ramp vehicles, and minimum gap for lateral movements. A wide distribution of desired vehicle speeds (ranging from 60 – 100

kmph) is used to produce different free-flow wave propagation velocities as is the case for heterogeneous traffic.

We simulate three traffic scenarios with different input vehicle demand profiles on the freeway segment: 800-1200 vehs/hr, 2400-3000 vehs/hr, and 4200-5400 vehs/hr. We used these demand profiles to replicate distinct traffic conditions on the simulated freeway, namely free-flowing, slow-moving (moderately congested), and (heavily) congested traffic. We used on-ramp inflows that constitute 15-20% of the total freeway flows. Each traffic scenario is simulated for 2 hrs and the vehicle trajectory data for an 800 m homogeneous section on the freeway is recorded. The trajectory data corresponding to three traffic scenarios and their traffic dynamics are summarized in Fig. 4.



(a) Space-time-speed contour plot.



(b) Flow-density scatter plot.

FIGURE 4: Visualization of the richness or the traffic features contained in the simulated training dataset (300-second snapshot).

Fig. 4(a) shows a 300 second snapshot of vehicle trajectories for the three simulated traffic scenarios. One can note the backward and forward propagating waves due to the stop-and-go, slow-moving, and heterogeneous free-flowing traffic (respectively) in Fig. 4(a). The anisotropic kernel is designed based on the range of wave propagation

velocities seen in these plots. Fig. 4(b) is a flow-density scatter-plot of the three scenarios. Together, these figures show the richness of traffic states contained in the training data. Later, we will use the flow-density scatter plot as a way to compare the traffic dynamics observed in the simulated and real-world traffic data.

3.2 Training procedure

The simulation output for each scenario is 7200 seconds of trajectory data for each of the three lanes. We first map the trajectories from a single lane onto a space-time plane to form an input and output frame of dimension 80×7200 (i.e., the mesh size is $10 \text{ m} \times 1 \text{ s}$). The PV trajectories for the input frame are selected at random using a 5% sampling rate. The output frame that forms the ground truth speed field is generated using the interpolation procedure described in eq. (6). We then extract samples of the input (\mathbf{z}^p) and output tensors (\mathbf{z}^f) from the input and output frames respectively, using a 80×60 sliding window. We generate 6000+ samples for each trajectory dataset using a 2 s spatial gap between sliding windows. We proceed similarly to generate more data with different sets of random input samples for each of the three traffic scenarios using a 5% sampling rate. The final augmented dataset has 64000+ input-output sample pairs for training the Deep CNN model. Note that the samples extracted from a specific trajectory record form a sequence, which violates the i.i.d assumption (independent and identically distributed) for the neural network training. However, this is rectified during the optimization stage, where only a randomly selected subset of the samples is used in each iteration of the CNN training (this is a common trick employed while training reinforcement learning models, for instance, the use of “replay memory” in [36]). We use the following additional parameters for training data generation: $|x| = 10 \text{ m}$, $|t| = 1 \text{ s}$, $c_w = 18 \text{ kmph}$, $c_v^{\max} = 100 \text{ kmph}$, $c_v^{\min} = 60 \text{ kmph}$, $V_{\max} = 95 \text{ kmph}$, $l_{\text{up}} = 80 \text{ m}$ and $l_{\text{dn}} = 40 \text{ m}$.

We train five instances of the anisotropic and isotropic CNN models, and report the average of their performance results. We use the *TensorFlow* framework [1] to train all the models. The two major hyper-parameters, namely the number of output filters and the kernel size in each layer, are independently optimized using the inbuilt *Hyperband* algorithm [28]. Other hyper-parameter choices are: gradient descent batch size: 32 samples, total training epochs: 300, (fixed) learning rate: $1e - 3$, and optimizer: Adam [22]. We use a GPU cluster with NVIDIA Tesla V100 32GB for training the models. The run time for a single training experiment is between 120 and 150 min. Note that the training can be viewed as an offline procedure.

3.3 Testing data

We test our model using three datasets: (i) a hold-out set from the simulated data that is not used for training (from a different lane of the freeway section), (ii) the Next Generation Simulation Program (NGSIM) dataset [52], and (iii) the recent highway drone (HighD) dataset [23]. The US-101 highway trajectory data from NGSIM contains the locations and speeds of all vehicles crossing the observed area during a 45 min time period with a 0.1 s resolution. The HighD data consists of trajectory data from several German highways, each consisting of a frame-wise recording of all vehicles passing a 400 m section during a 20 min duration, with a resolution of 25 frames/second. The input-output test samples are generated similarly to the training datasets with the respective space-time discretization parameters.

We emphasize that we do not use the NGSIM or HighD datasets for training the model. In other words, the model is trained with data from a simulation using a freeway in the United Arab Emirates; and then tested with additional data from that same simulation, as well as real data from a freeway in the United States and several freeways in Germany. This allows us to evaluate the model’s transferability to diverse traffic scenarios and dynamics not seen in the training set, and the viability of using simulated data instead of real data for training.

4 Results and Discussion

TABLE 1: Model architecture as obtained from the hyper-parameter optimization

Layer No.	Kernel size	Filter number
Conv-1	(5×5)	40
Conv-2	(7×7)	48
Conv-3	(7×7)	32
Conv-4	(5×5)	48
Conv-5	(5×5)	40
Conv-6	(9×9)	56
Output	(7×7)	1

In this section, we present the anisotropic reconstruction results and compare the isotropic and anisotropic models. We also discuss the transferability of the trained models to real-world traffic conditions and extend the results to handle varying PV penetration rates.

The architecture of the CNN model obtained from the hyper-parameter optimization is shown in Table 1. We use the same optimized architecture for both the anisotropic and isotropic CNN models.

TABLE 2: Comparison of anisotropic and isotropic models. Percent change is with respect to isotropic model.

Metric		Isotropic model	Anisotropic model	Percent change
Root mean squared error (<i>kmph</i>)	Congested	8.60 (+/- 3.16)	8.50 (+/- 3.15)	-1.2%
	Slow-moving	10.37 (+/- 1.60)	10.53 (+/- 1.70)	+1.5%
	Free-flowing	7.42 (+/- 2.23)	7.40 (+/- 2.22)	-0.3%
	Total	8.71 (+/- 2.76)	8.76 (+/- 2.71)	+0.5%
Number of parameters		443193	215625	-51.4%

4.1 Anisotropic CNN model reconstruction

Fig. 5 shows five sample estimated speed fields from the hold-out simulated test dataset using the anisotropic model. The reconstruction window is $800 \text{ m} \times 60 \text{ s}$ with a $10 \text{ m} \times 1 \text{ s}$ resolution. The true speed field, PV trajectories, and speed profiles at three time instants ($t = 10, 30,$ and 50 s) are also shown for each sample. Three of the samples correspond to congested traffic conditions, one corresponds to slow-moving traffic conditions, and one corresponds to free-flowing traffic conditions.

There are several points of interest to note about the reconstruction: All the estimated speed fields are feasible in terms of traffic physics and capture the different traffic states well. The model reproduces the existence of free-flow, congested and transition traffic dynamics correctly despite having very limited input information from the PV trajectories. One can observe the accurate prediction of shockwave dynamics in the congested traffic samples (a)-(c). This is also evident from the speed profile comparison. The true speed profile is often noisy, and the reconstruction has a smoothing effect due to the local convolutional operations in the CNN layers.

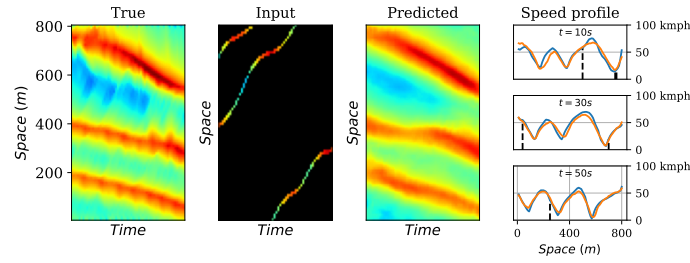
We have observed that the estimated speeds in slow-moving traffic have a higher root mean squared error (RMSE) than those in congested and free-flowing traffic; see Fig. 5 (d)-(e) and Table 2. In slow-moving traffic, heterogeneity (caused by different vehicle characteristics, driving behaviors, etc.) is predominant, and one can see different forward wave propagation velocities in the speed field; see the example in Fig. 5 (d). Therefore, estimation is inherently a challenging problem unless we observe the actual travel speed. This is not the case for congested traffic, where the collective dynamics can be inferred from the trajectory of a single vehicle, or for free-flowing traffic, where

the traffic heterogeneity is limited. In short, traffic speed fields with varied forward propagation wave velocities are still difficult to infer. Interestingly, in all the scenarios, the anisotropic model predicts the average desired vehicle speed in areas where there are no PV trajectories, which is a reasonable conclusion when no vehicles are observed.

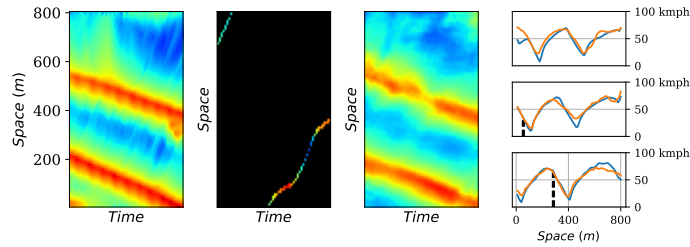
One has to look at these estimation results as a spatio-temporal traffic wave reconstruction from the available sparse trajectories over space and time. Traditional Kalman Filter based assimilation techniques only exploit state information from one (or a few) time step(s) when estimating the traffic speeds. This is inefficient in terms of data usage and fails to accurately reconstruct the dynamics. Furthermore, we have tuned the Deep CNN model architecture to learn different traffic wave dynamics. Whether to produce a backward or forward wave depends on the traffic regime, which the model infers from the input trajectories. This is confirmed from the latent space projection of the data (i.e., the output from the encoder model), where three distinct clusters were generated, corresponding to free-flowing, slow-moving and congested traffic, respectively. Another way to put this is that a neural network model can solve an under-determined system - a major upside compared to other machine learning models. This is in contrast with traditional estimation methods which require additional information on initial/boundary conditions or traffic demands.

4.2 Comparison of anisotropic and isotropic models

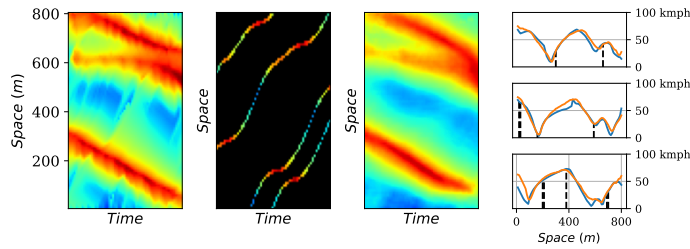
We next compare the performance and computational requirements of the anisotropic and isotropic models in Table 2. The RMSE calculation shown in the table is the sample average for 4000+ simulated test samples. Overall, the anisotropic and isotropic models have similar per-



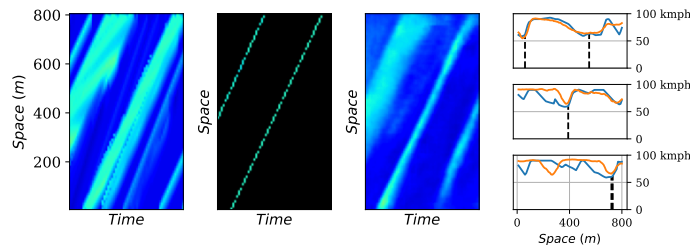
(a) Congested traffic, RMSE = 5.34 kmph



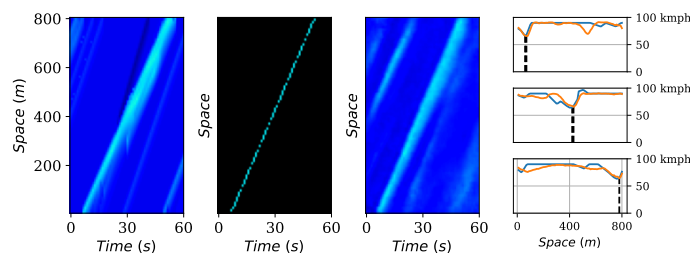
(b) Congested traffic, RMSE = 7.84 kmph



(c) Congested traffic, RMSE = 6.36 kmph



(d) Slow-moving traffic, RMSE = 10.78 kmph



(e) Free-flowing traffic, RMSE = 5.54 kmph

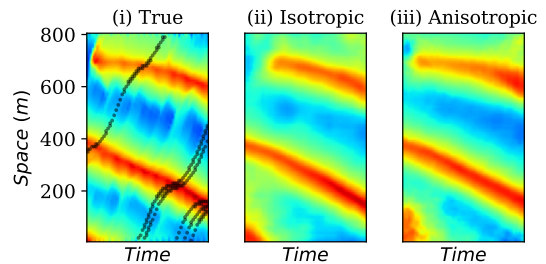
FIGURE 5: Estimated speed field for selected samples in the simulated test data using the anisotropic CNN model. The fourth column shows the speed profile across the road section at $t = 10, 30,$ and 50 secs (*blue - true speeds, orange - estimated speeds, black vertical dashed line - probe vehicle speed*).

formance in terms of accuracy, but the anisotropic model leads to more physically plausible shockwave dynamics (this is discussed below). In particular, the anisotropic model performs slightly better in estimating the congested and free-flowing traffic as expected, however, it is worse in predicting the slow-moving traffic. This is because the slow-moving data samples comprise heterogeneous traffic in the free-flow regime, which might be better observed by an isotropic kernel than a restricted anisotropic kernel. Depending on the desired speed distribution, one can increase the extent of the anisotropic kernel and rectify this.

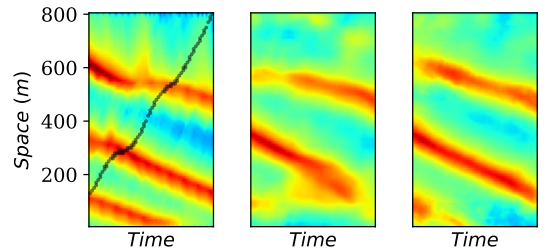
Table 2 also shows that the anisotropic model requires only half as many parameters as the isotropic model, which is a significant improvement in model complexity given that the performance of the two models is very similar. From a computational perspective, this is a substantial advantage, leading to faster model convergence (RMSE reduction per training epoch) and a potential reduction in the number of training samples required. This confirms that exploiting domain knowledge results in simpler and more interpretable learning models. It also complements the result of van Lint *et al.* [54], where the authors eliminated the least significant parameters from a neural network model for TSE, and found the remaining network represents correlations that are in accordance with traffic principles.

Although the isotropic and anisotropic models perform comparably in terms of the average error in estimating the speed, there are some examples where they differ in terms of the structure (speed and extent) of the shockwaves they produce. This is illustrated in Fig. 6, which shows certain examples where the anisotropic model clearly reconstructs more physically plausible shockwave dynamics, as mentioned below.

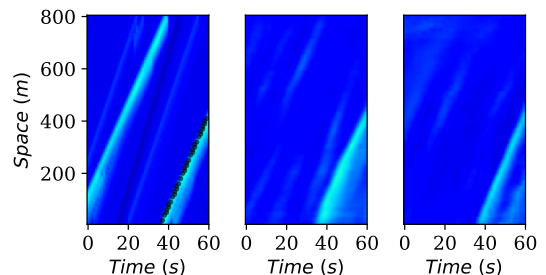
In the example in Fig. 6(a), the isotropic CNN underestimates the length of the shockwave at the top, whereas the anisotropic CNN correctly predicts that it existed some time prior to the two PV trajectories crossing it. This is because the anisotropic kernel gets more activation along the direction of the shockwave and hence reconstructs the stop-and-go region correctly, whereas the isotropic kernel considers all directions, which possibly results in averaging out all the nearby activations. Similar patterns have been observed in other test instances. The estimation in Fig. 6(b) is obtained using a single input trajectory. The anisotropic model gives a plausible reconstruction of the shockwave whereas the isotropic reconstruction shows large dispersion, which is also physically inconsistent with the input data. The design of anisotropic kernels can rule out such inconsistencies arising in the estimation. Fig. 6(c) shows a free-flowing traffic estimation. Again the



(a) Example 1 (Congested traffic, RMSE = 5.34 kmph)



(b) Example 2 (Congested traffic, RMSE = 7.84 kmph)



(c) Example 3 (Free-flowing traffic, RMSE = 6.36 kmph)

FIGURE 6: Estimated speed fields for some selected samples in the simulated test data using the anisotropic and the isotropic CNN models. Black lines show the probe vehicle trajectories used for the reconstruction.

forward wave produced by the isotropic kernel has more dispersion. In summary, one can see that the anisotropic model produces more accurate wave propagation dynamics consistent with traffic physics, even though the RMSEs of the models are similar.

4.3 Transferability to real-world traffic dynamics

To understand how well the anisotropic CNN model performs in scenarios with different traffic characteristics than those observed in the training dataset, we test it on various real-world freeway sections. Figs. 7 to 9 show the estimation results for three sample freeway sections from the HighD and NGSIM datasets using data with a PV

sampling rate of 5%.

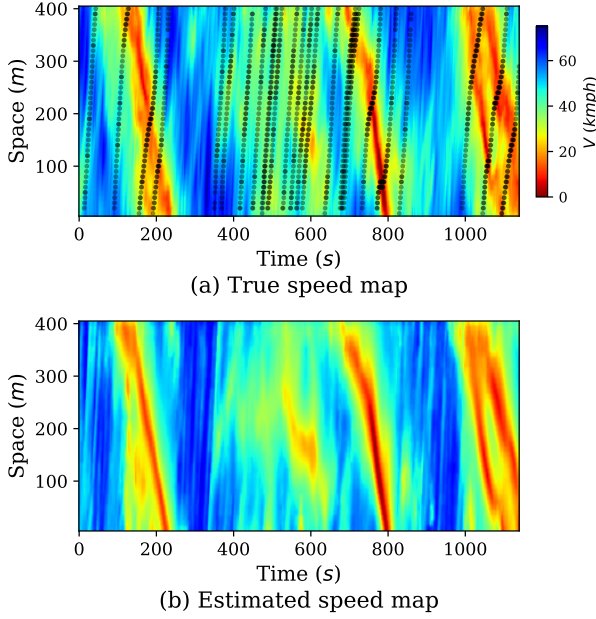


FIGURE 7: Estimated speed field of lane 4 of highway No. 25 in the HighD dataset using 5% probe sampling rate. The road section is $X = 400$ m long and the reconstruction period is $T = 1140$ s. The RMSE is 6.80 kmph.

A quick observation shows that all three example reconstructions are plausible, despite having different space-time dimensions from those used in the training dataset. This is possible because of the parameter sharing property of CNNs, whereby the features learned during training (traffic characteristics in this case) are space-time invariant, and hence can be used with any spatio-temporal reconstruction window.

Closer observation reveals variation in the performance across the three examples. The estimated speed field in Fig. 7 has the lowest RMSE (≈ 6.80 kmph), and the speed, width and duration of the predicted backward propagating shockwaves are accurate. In the estimation in Fig. 8, the shockwave reconstruction and speeds are reasonably correct, and the RMSE is moderate (≈ 10.50 kmph). The model correctly predicts the dissipation of the shockwaves during the initial 600 seconds, but fails to accurately determine the width of shockwaves later on. The third freeway section, shown in Fig. 9, comprises free-flowing traffic and has the highest RMSE (≈ 14.60 kmph). Apart from the inherent difficulties in the estimation of free-flowing traffic speeds, one can also observe that the speed of forward waves predicted by the model is slightly lower than that from the true waves; see the slow-moving band around

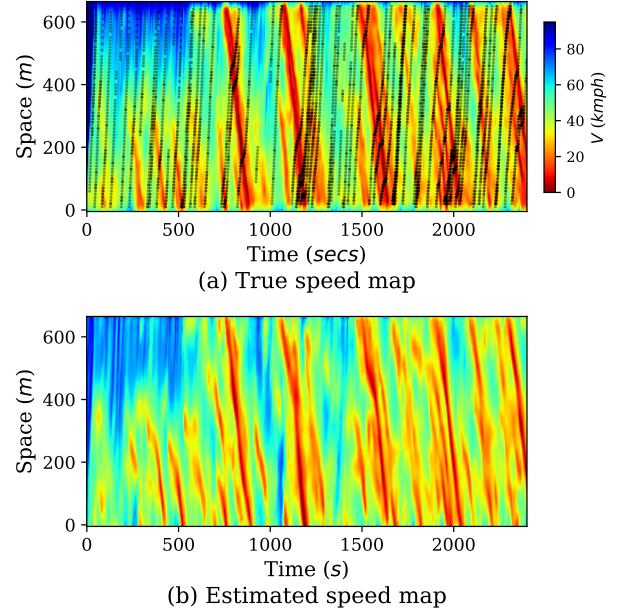


FIGURE 8: Estimated speed field of lane 2 of U.S. Highway 101 in the NGSIM dataset using 5% probe sampling rate. The road section is $X = 670$ m long and the reconstruction period is $T = 2400$ s. The RMSE is 10.50 kmph.

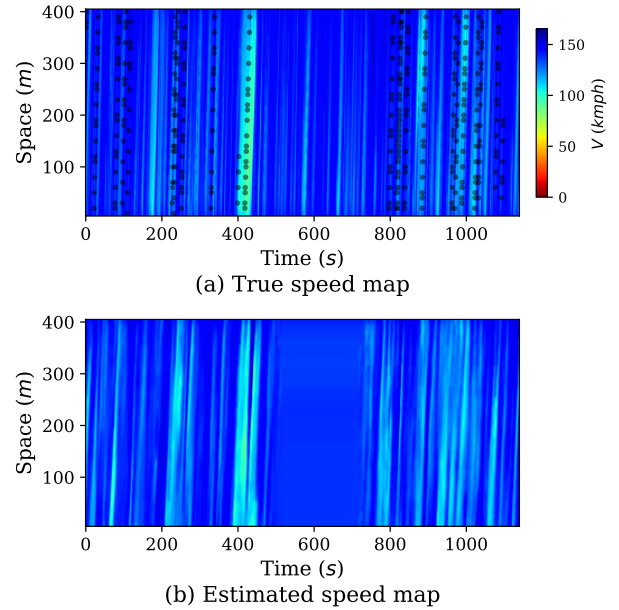


FIGURE 9: Estimated speed field of lane 6 of Highway No. 44 in the HighD dataset using 5% probe sampling rate. The road section is $X = 400$ m long and the reconstruction period is $T = 1140$ s. The RMSE is 14.60 kmph.

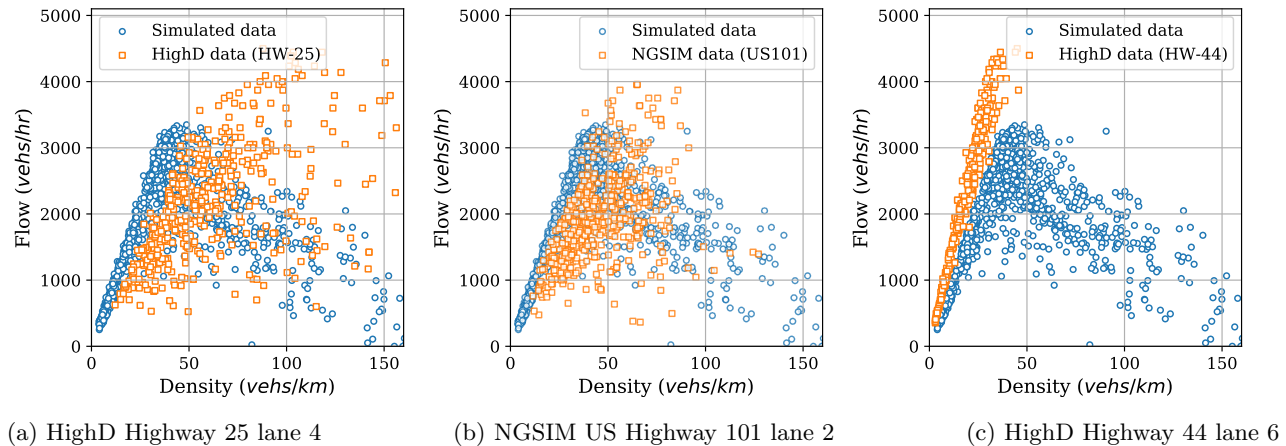


FIGURE 10: Flow-density scatter plot comparing the traffic characteristics of the real-world datasets with the simulated training data

400 secs as an example. This is due to the difference in the traffic characteristics in the training and testing data, which we elaborate on below.

Recall that the CNN model trained on the simulated data encompasses the knowledge of traffic dynamics of a specific freeway section. How well this model transfers to other test scenarios depends on the traffic characteristics of the test segment. One can explain the difference in the RMSE errors in Figs. 7 to 9 by comparing the dynamics contained in the simulated data and the test data. One useful tool for this comparison is the flow-density scatter plot, which is shown in Fig. 10. The reason for the low RMSE in the first two examples is that the freeways are operating in the congested regime and the shockwave speeds in the simulated and test data are similar. Likewise, the reason for slightly lower prediction of free-flowing speed in the third freeway section (which operates in free-flowing traffic) is evident from Fig. 10(c). A similar reasoning is applicable when one discusses the transferability of the simulated section with its own real-world section, as the simulation doesn't capture the complete dynamics. Note that we don't assume a fundamental diagram (FD); instead, we use it as a tool to demonstrate the richness of the data. Empirical FD comparisons can be further exploited to calibrate the trained deep learning model to match with the traffic dynamics of the test data. This is beyond the scope of the current work and represents a possible future extension.

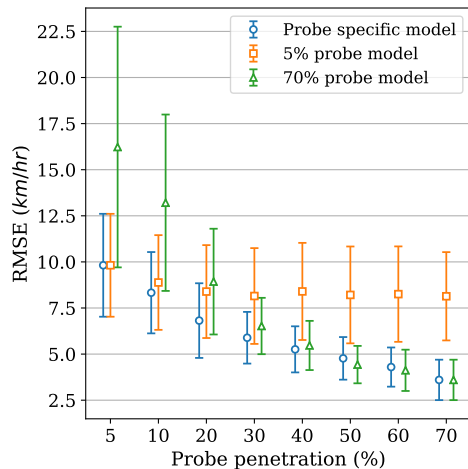
4.4 Variable probe vehicle penetration rates

To conclude our evaluation of the CNN model's performance, we investigate the effect of increasing the PV penetration rate beyond 5%. We train six sepa-

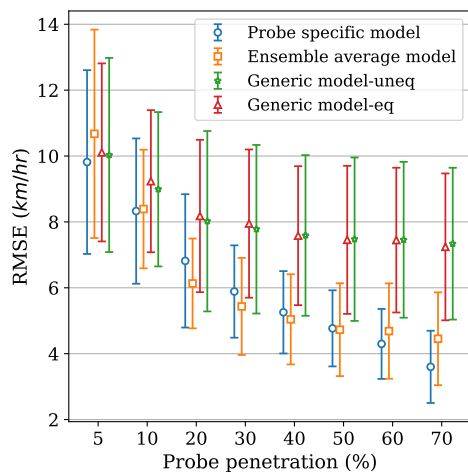
rate models using data with specific penetration rates: 10%, 20%, ..., 70%. The respective input PV trajectory data are generated in the same way as the 5% data, as explained in Sec. 3 B. The average RMSE results for these models (along with the original 5% model) are shown in Fig. 11(a) (labeled *probe specific models*). As expected, the RMSE decreases with higher penetration rates. However, it is interesting to note that these probe specific models are not trivially generalizable to handle penetration rates other than what they were trained on, i.e., the models are penetration rate dependent. This is demonstrated further in Fig. 11(a), where we have tested the model trained on 5% PV penetration with higher penetration rates (labeled *5% probe model*) and vice-versa with the model trained on 70% PV penetration (labeled *70% probe model*). It is clear that these probe specific models perform well only in their domain. This is because of the unconstrained latent space representation while training the CNN models, and is inevitable in any data driven models unless physical constraints are imposed.

The actual PV penetration rate depends on the prevailing traffic demand on the freeway, which is hard to measure in practice. We aim for an estimation model that performs well irrespective of the penetration rate. Therefore, we test three methods to handle varying penetration rates. The first two methods are brute force approaches, which consist of training the CNN model on a dataset containing the whole range of PV penetrations 5%, 10%, 20%, ..., 70%. The third method is to use an ensemble CNN model. The RMSE results from these models are compared in Fig. 11(b).

The first model (labeled *generic model-eq*) is trained on a dataset consisting of all PV penetration rates in equal



(a) Probe specific models



(b) Generic models

FIGURE 11: Probe vehicle penetration analysis

proportion. The second model (labeled *generic model-uneq*) is similar except that we give more importance to lower PV penetration rates which are more difficult to learn. This is achieved by including more data samples for lower PV penetration rates. Both these models, however, perform sub-optimally compared to the probe specific models. The best method is the ensemble CNN model, which takes the average of the predictions of all the probe specific models. This method performs consistently well across all the PV penetration rates, even outperforming the respective probe specific models in certain cases. In addition to the performance, another advantage of the ensemble model compared to the generic models is that each probe specific component of the ensemble can be in-

dependently trained, enabling the training to be conducted in a distributed manner.

5 Conclusion

In this paper, we propose a learning based speed field estimation method which incorporates the wave propagation characteristics of traffic. Our model combines the advantages and mitigates the disadvantages of the two main approaches to traffic state estimation: (i) applying naïve (vanilla) learning models which do not guarantee feasible solutions and are difficult to interpret and analyze due to their black box nature, and (ii) developing parametric traffic physics based models which have several assumptions and transferability issues. Our approach allows us to use data-driven learning techniques while honoring well established (empirical and theoretical) features of traffic.

Our speed reconstruction model is a Deep Convolutional Neural Network (Deep CNN) which uses sparse probe vehicle (PV) trajectory observations (with a penetration rate as low as 5%) to predict the speed field over a given space-time plane with fine resolution. The CNN uses an anisotropic kernel which is designed to capture information from the relevant directions in free-flowing and congested traffic. This anisotropic model also significantly reduces the computational cost in comparison to an isotropic model. We train the model using simulated traffic data under various demand conditions, in order to implicitly incorporate the dynamics of the traffic flow model used in the simulation, and test it using real data from multiple datasets. Our results show that the anisotropic CNN performs well in terms of estimation error, given the sparsity of the PV trajectories. We present examples where it is clearly visible how the anisotropic kernel aids the CNN in reconstructing the duration and dispersion of shockwaves more accurately than the isotropic CNN. We also show that the model transfers well to real traffic with varied characteristics, despite being trained exclusively on simulated traffic. Finally, we propose a method to allow the model to adjust to multiple and unknown PV penetration levels.

We believe that the optimal way to apply learning techniques to a specific domain such as traffic state estimation is to integrate the fundamental principles of the domain into the framework of the learning model. This paper represents only one possible example of this general approach. In future work, we aim to explore other methods to incorporate traffic flow theory into learning models such as CNNs.

Acknowledgment

This work was supported by the NYUAD Center for Interacting Urban Networks (CITIES), funded by Tamkeen under the NYUAD Research Institute Award CG001 and by the Swiss Re Institute under the Quantum CitiesTM initiative. The views expressed in this article are those of the author and do not reflect the opinions of CITIES or its funders.

References

- [1] Martín Abadi, Paul Barham, Jianmin Chen, Zhifeng Chen, Andy Davis, Jeffrey Dean, Matthieu Devin, Sanjay Ghemawat, Geoffrey Irving, Michael Isard, et al. Tensorflow: A system for large-scale machine learning. In *12th {USENIX} symposium on operating systems design and implementation ({OSDI} 16)*, pages 265–283, 2016.
- [2] A. Aw and Michel Rascole. Resurrection of “second order” models of traffic flow. *SIAM Journal on Applied Mathematics*, 60(3):916–938, 2000.
- [3] Nikolaos Bekiaris-Liberis, Claudio Roncoli, and Markos Papageorgiou. Highway traffic state estimation with mixed connected and conventional vehicles. *IEEE Transactions on Intelligent Transportation Systems*, 17(12):3484–3497, 2016.
- [4] Nikolaos Bekiaris-Liberis, Claudio Roncoli, and Markos Papageorgiou. Highway traffic state estimation per lane in the presence of connected vehicles. *Transportation research part B: methodological*, 106: 1–28, 2017.
- [5] Ouafa Benkraouda, Bilal Thonnam Thodi, Hwasoo Yeo, Monica Menendez, and Saif Eddin Jabari. Traffic data imputation using deep convolutional neural networks. *IEEE Access*, 8:104740–104752, 2020.
- [6] C. Daganzo and M. Menéndez. A variational formulation of kinematic waves: Bottleneck properties and examples. In *16th International Symposium on Transportation and Traffic Theory*, 2005.
- [7] Carlos F. Daganzo. Requiem for second-order fluid approximations of traffic flow. *Transportation Research Part B: Methodological*, 29(4):277 – 286, 1995. ISSN 0191-2615. doi: [https://doi.org/10.1016/0191-2615\(95\)00007-Z](https://doi.org/10.1016/0191-2615(95)00007-Z). URL <http://www.sciencedirect.com/science/article/pii/019126159500007Z>.
- [8] Carlos F. Daganzo. A variational formulation of kinematic waves: basic theory and complex boundary conditions. *Transportation Research Part B: Methodological*, 39(2):187 – 196, 2005. ISSN 0191-2615. doi: <https://doi.org/10.1016/j.trb.2004.04.003>. URL <http://www.sciencedirect.com/science/article/pii/S0191261504000487>.
- [9] Igor Dakic and Monica Menendez. On the use of lagrangian observations from public transport and probe vehicles to estimate car space-mean speeds in bi-modal urban networks. *Transportation Research Part C: Emerging Technologies*, 91:317 – 334, 2018. ISSN 0968-090X. doi: <https://doi.org/10.1016/j.trc.2018.04.004>.
- [10] Leslie C. Edie. *Discussion of traffic stream measurements and definitions*. Port of New York Authority and International Symposium on the Theory of Road Traffic Flow, New York, 1963.
- [11] S. Guler, M. Menendez, and L. Meier. Using connected vehicle technology to improve the efficiency of intersections. *Transportation Research Part C: Emerging Technologies*, 46:121–131, 2014.
- [12] Ayalew Belay Habtie, Ajith Abraham, and Dida Midekso. Artificial neural network based real-time urban road traffic state estimation framework. In *Computational Intelligence in Wireless Sensor Networks*, pages 73–97. Springer, 2017.
- [13] Benjamin Hamner. Predicting travel times with context-dependent random forests by modeling local and aggregate traffic flow. In *2010 IEEE International Conference on Data Mining Workshops*, pages 1357–1359. IEEE, 2010.
- [14] Jiheng Huang and Shaurya Agarwal. Physics informed deep learning for traffic state estimation. In *IEEE Intelligent Transportation Systems Conference*, 2020.
- [15] S.E. Jabari and H. Liu. A stochastic model of traffic flow: Theoretical foundations. *Transportation Research Part B: Methodological*, 46(1):156–174, 2012.
- [16] S.E. Jabari and H. Liu. A stochastic model of traffic flow: Gaussian approximation and estimation. *Transportation Research Part B: Methodological*, 47:15–41, 2013.
- [17] S.E. Jabari, F. Zheng, H. Liu, and M. Filipovska. Stochastic Lagrangian modeling of traffic dynamics. In *The 97th Annual Meeting of the Transportation*

- Research Board, Washington D.C.*, pages 18–04170, 2018.
- [18] S.E. Jabari, D. Dilip, D. Lin, and B. Thonnam Thodi. Learning traffic flow dynamics using random fields. *IEEE Access*, 7:130566–130577, 2019.
- [19] S.E. Jabari, N. Freris, and D. Dilip. Sparse travel time estimation from streaming data. *Transportation Science*, 54(1):1–20, 2020.
- [20] Y. Jia, J. Wu, and Y. Du. Traffic speed prediction using deep learning method. In *2016 IEEE 19th International Conference on Intelligent Transportation Systems (ITSC)*, pages 1217–1222, 2016.
- [21] Sakib Mahmud Khan, Kakan C Dey, and Mashrur Chowdhury. Real-time traffic state estimation with connected vehicles. *IEEE Transactions on Intelligent Transportation Systems*, 18(7):1687–1699, 2017.
- [22] D. Kingma and J. Ba. Adam: A method for stochastic optimization. *arXiv preprint arXiv:1412.6980*, 2014.
- [23] Robert Krajewski, Julian Bock, Laurent Kloeker, and Lutz Eckstein. The highd dataset: A drone dataset of naturalistic vehicle trajectories on german highways for validation of highly automated driving systems. In *2018 21st International Conference on Intelligent Transportation Systems (ITSC)*, pages 2118–2125. IEEE, 2018.
- [24] Ibai Laña, Jesus L Lobo, Elisa Capecci, Javier Del Ser, and Nikola Kasabov. Adaptive long-term traffic state estimation with evolving spiking neural networks. *Transportation Research Part C: Emerging Technologies*, 101:126–144, 2019.
- [25] L. Li and S.E. Jabari. Position weighted backpressure intersection control for urban networks. *Transportation Research Part B: Methodological*, 128:435–461, 2019.
- [26] Li Li, Yuebiao Li, and Zhiheng Li. Efficient missing data imputing for traffic flow by considering temporal and spatial dependence. *Transportation research part C: emerging technologies*, 34:108–120, 2013.
- [27] Li Li, Victor Okoth, and Saif Eddin Jabari. Backpressure control with estimated queue lengths for urban network traffic. *IET Intelligent Transport Systems*, in press:DOI: 10.1049/itr2.12027, 2021.
- [28] Lisha Li, Kevin Jamieson, Giulia DeSalvo, Afshin Rostamizadeh, and Ameet Talwalkar. Hyperband: A novel bandit-based approach to hyperparameter optimization. *Journal of Machine Learning Research*, 18(185):1–52, 2018. URL <http://jmlr.org/papers/v18/16-558.html>.
- [29] Wenqing Li, Chuhan Yang, and Saif Eddin Jabari. Nonlinear traffic prediction as a matrix completion problem with ensemble learning. *arXiv preprint arXiv:2001.02492*, 2020.
- [30] Wenqing Li, Chuhan Yang, and Saif Eddin Jabari. Short-term traffic forecasting using high-resolution traffic data. In *2020 IEEE 23rd International Conference on Intelligent Transportation Systems (ITSC)*, pages 1–6. IEEE, 2020.
- [31] Michael James Lighthill and Gerald Beresford Whitham. On kinematic waves ii. a theory of traffic flow on long crowded roads. *Proceedings of the Royal Society of London. Series A. Mathematical and Physical Sciences*, 229(1178):317–345, 1955.
- [32] DianChao Lin and Saif Eddin Jabari. Pay for intersection priority: A free market mechanism for connected vehicles. *IEEE Transactions on Intelligent Transportation Systems*, pages 1–12, 2021. doi: 10.1109/TITS.2020.3048475.
- [33] John Liu, Matthieu Barreau, and Karl H Johansson. Learning-based traffic state reconstruction using probe vehicles. *arXiv preprint arXiv:2011.05031*, 2020.
- [34] X. Ma, Z. Tao, Y. Wang, H. Yu, and Y. Wang. Long short-term memory neural network for traffic speed prediction using remote microwave sensor data. *Transportation Research Part C: Emerging Technologies*, 54:187–197, 2015.
- [35] Xiaolei Ma, Chuan Ding, Sen Luan, Yong Wang, and Yunpeng Wang. Prioritizing influential factors for freeway incident clearance time prediction using the gradient boosting decision trees method. *IEEE Transactions on Intelligent Transportation Systems*, 18(9): 2303–2310, 2017.
- [36] Volodymyr Mnih, Koray Kavukcuoglu, David Silver, Andrei A. Rusu, Joel Veness, Marc G. Bellemare, Alex Graves, Martin Riedmiller, Andreas K. Fidjeland, Georg Ostrovski, Stig Petersen, Charles Beattie, Amir Sadik, Ioannis Antonoglou, Helen King, Dharshan Kumaran, Daan Wierstra, Shane Legg, and Demis Hassabis. Human-level control through

- deep reinforcement learning. *Nature*, 518(7540):529–533, February 2015. ISSN 00280836. URL <http://dx.doi.org/10.1038/nature14236>.
- [37] Alfredo Nantes, Dong Ngoduy, Ashish Bhaskar, Marc Miska, and Edward Chung. Real-time traffic state estimation in urban corridors from heterogeneous data. *Transportation Research Part C: Emerging Technologies*, 66:99–118, 2016.
- [38] Gordon F Newell. A simplified theory of kinematic waves in highway traffic, part i: General theory. *Transportation Research Part B: Methodological*, 27(4):281–287, 1993.
- [39] Markos Papageorgiou. Overview of road traffic control strategies. *IFAC Proceedings Volumes*, 37(19):29–40, 2004.
- [40] N. Polson and V. Sokolov. Deep learning for short-term traffic flow prediction. *Transportation Research Part C: Emerging Technologies*, 79:1–17, 2017.
- [41] Maziar Raissi, Paris Perdikaris, and George E Karniadakis. Physics-informed neural networks: A deep learning framework for solving forward and inverse problems involving nonlinear partial differential equations. *Journal of Computational Physics*, 378:686–707, 2019.
- [42] Paul I Richards. Shock waves on the highway. *Operations research*, 4(1):42–51, 1956.
- [43] Majid Rostami-Shahrabaki, Ali Akbar Safavi, Markos Papageorgiou, Peyman Setoodeh, and Ioannis Papamichail. State estimation in urban traffic networks: A two-layer approach. *Transportation Research Part C: Emerging Technologies*, 115:102616, 2020. ISSN 0968-090X. doi: <https://doi.org/10.1016/j.trc.2020.102616>.
- [44] T. Seo, A. Bayen, T. Kusakabe, and Y. Asakura. Traffic state estimation on highway: A comprehensive survey. *Annual Reviews in Control*, 43:128–151, 2017.
- [45] Seongmoon Kim, M. E. Lewis, and C. C. White. Optimal vehicle routing with real-time traffic information. *IEEE Transactions on Intelligent Transportation Systems*, 6(2):178–188, 2005. doi: 10.1109/TITS.2005.848362.
- [46] Rongye Shi, Zhaobin Mo, and Xuan Di. Physics-informed deep learning for traffic state estimation: A hybrid paradigm informed by second-order traffic models. In *AAAI*, pages 3617–3621, 2021.
- [47] J. Tobin, R. Fong, A. Ray, J. Schneider, W. Zaremba, and P. Abbeel. Domain randomization for transferring deep neural networks from simulation to the real world. In *2017 IEEE/RSJ International Conference on Intelligent Robots and Systems (IROS)*, pages 23–30, 2017. doi: 10.1109/IROS.2017.8202133.
- [48] M. Treiber and D. Helbing. Reconstructing the spatio-temporal traffic dynamics from stationary detector data. *Cooper@tive Tr@nsport@tion Dyn@mics*, 1(3):3–1, 2002.
- [49] M. Treiber and A. Kesting. *Traffic Flow Dynamics: Data, Models, and Simulation*. Springer-Verlag, Berlin, 2013.
- [50] Martin Treiber, Arne Kesting, and R. Eddie Wilson. Reconstructing the traffic state by fusion of heterogeneous data. *Computer-Aided Civil and Infrastructure Engineering*, 26(6):408–419, 2011.
- [51] J. Tremblay, A. Prakash, D. Acuna, M. Brophy, V. Jampani, C. Anil, T. To, E. Cameracci, S. Bochoon, and S. Birchfield. Training deep networks with synthetic data: Bridging the reality gap by domain randomization. In *2018 IEEE/CVF Conference on Computer Vision and Pattern Recognition Workshops (CVPRW)*, pages 1082–10828, 2018. doi: 10.1109/CVPRW.2018.00143.
- [52] United States Department of Transportation. NGSIM—Next Generation Simulation, 2006. URL <https://ops.fhwa.dot.gov/trafficanalysistools/ngsim.htm>.
- [53] Paul B.C. van Erp, Victor L. Knoop, and Serge P. Hoogendoorn. On the value of relative flow data. *Transportation Research Part C: Emerging Technologies*, 113:74 – 90, 2020. doi: <https://doi.org/10.1016/j.trc.2019.05.001>.
- [54] JWC Van Lint, SP Hoogendoorn, and Henk J van Zuylen. Freeway travel time prediction with state-space neural networks: modeling state-space dynamics with recurrent neural networks. *Transportation Research Record*, 1811(1):30–39, 2002.
- [55] Femke van Wageningen-Kessels, Bas van’t Hof, Serge P. Hoogendoorn, Hans van Lint, and Kees Vuik. Anisotropy in generic multi-class traffic flow models. *Transportmetrica A: Transport Science*, 9(5):451–472, 2013. doi: 10.1080/18128602.2011.596289. URL <https://doi.org/10.1080/18128602.2011.596289>.

- [56] J. Wang, Q. Gu, J. Wu, G. Liu, and Z. Xiong. Traffic speed prediction and congestion source exploration: A deep learning method. In *2016 IEEE 16th International Conference on Data Mining (ICDM)*, pages 499–508, 2016.
- [57] Jin Wang and Qixin Shi. Short-term traffic speed forecasting hybrid model based on chaos-wavelet analysis-support vector machine theory. *Transportation Research Part C: Emerging Technologies*, 27:219–232, 2013.
- [58] Yibing Wang and Markos Papageorgiou. Real-time freeway traffic state estimation based on extended kalman filter: a general approach. *Transportation Research Part B: Methodological*, 39(2):141 – 167, 2005. ISSN 0191-2615. doi: <https://doi.org/10.1016/j.trb.2004.03.003>. URL <http://www.sciencedirect.com/science/article/pii/S0191261504000438>.
- [59] Jianli Xiao, Chao Wei, and Yuncai Liu. Speed estimation of traffic flow using multiple kernel support vector regression. *Physica A: Statistical Mechanics and its Applications*, 509:989–997, 2018.
- [60] K. Yang and M. Menendez. Queue estimation in a connected vehicle environment: A convex approach. *IEEE Transactions on Intelligent Transportation Systems*, 20(7):2480–2496, 2019.
- [61] Kaidi Yang, S. Ilgin Guler, and Monica Menendez. Isolated intersection control for various levels of vehicle technology: Conventional, connected, and automated vehicles. *Transportation Research Part C: Emerging Technologies*, 72:109 – 129, 2016. ISSN 0968-090X. doi: <https://doi.org/10.1016/j.trc.2016.08.009>. URL <http://www.sciencedirect.com/science/article/pii/S0968090X16301437>.
- [62] Kaidi Yang, Nan Zheng, and Monica Menendez. Multi-scale perimeter control approach in a connected-vehicle environment. *Transportation Research Procedia*, 23:101 – 120, 2017. ISSN 2352-1465. doi: <https://doi.org/10.1016/j.trpro.2017.05.007>.
- [63] Y. Yuan, J. W. C. van Lint, R. E. Wilson, F. van Wageningen-Kessels, and S. P. Hoogendoorn. Real-time lagrangian traffic state estimator for freeways. *IEEE Transactions on Intelligent Transportation Systems*, 13(1):59–70, 2012. doi: 10.1109/TITS.2011.2178837.
- [64] H Michael Zhang. A non-equilibrium traffic model devoid of gas-like behavior. *Transportation Research Part B: Methodological*, 36(3):275–290, 2002.
- [65] Yanru Zhang and Ali Haghani. A gradient boosting method to improve travel time prediction. *Transportation Research Part C: Emerging Technologies*, 58:308–324, 2015.
- [66] Zhao Zhang, Yun Yuan, and Xianfeng Yang. A hybrid machine learning approach for freeway traffic speed estimation. *Transportation research record*, 2674(10): 68–78, 2020.
- [67] Z. Zhao, Z. Wang, G. Wu, F. Ye, and M. J. Barth. The state-of-the-art of coordinated ramp control with mixed traffic conditions. In *2019 IEEE Intelligent Transportation Systems Conference (ITSC)*, pages 1741–1748, 2019. doi: 10.1109/ITSC.2019.8917067.
- [68] F. Zheng, S.E. Jabari, H. Liu, and D. Lin. Traffic state estimation using stochastic Lagrangian dynamics. *Transportation Research Part B: Methodological*, 115:143–165, 2018.